ESOC ACTIVITIES DURING THE MIR DE-ORBIT

H. Klinkrad, W. Flury, C. Hernández, M. Landgraf, R. Jehn, U. Christ and F. Sintoni

ESA/ESOC, D-64293 Darmstadt, Germany

ABSTRACT

On March 23, 2001, Mir was de-orbited in a controlled fashion, following a successful mission of 15 years. The de-orbiting operations were conducted by the TsUP Mission Control Center, who also consulted entities outside Russia, in order to consolidate their knowledge on the Mir orbit and attitude prior to the initiation of the de-orbit sequence. The European Space Agency ESA through their operations centre ESOC was tasked to support the pre-entry analysis of TsUP by own results, and by routing of Russian and European data via a dedicated communications network. Analysis results produced by ESOC, and details on the data exchange will be highlighted in this paper. The Mir de-orbit and its assessed risk potential will also be compared with the re-entries of Skylab and Salyut-7/Kosmos-1686.

1. INTRODUCTION

The assembly of the Mir space station started with the launch of its core module on 19 Feb 1986, followed by the launches of Kvant (Mar 1987), Kvant-2 (Dec 1989), Crystal (Jun 1990), Spectr (Jun 1995), and Priroda (Apr 1996). As part of the ISS Phase 1 mission (STS74), also a docking module for STS was installed on Crystal (Nov 1995), which was subsequently used during 10 visits by the Space Shuttle. The total Mir assembly in its final de-orbit configuration on 23 Mar 2001 had a mass of about 135 tonnes, a volume of 400 m^3, and dimensions of some 30 to 33 meters along each of the main axes. It was the largest re-entering, man-made object to date. During its continuous mission of 15 years Mir was visited by 71 cosmonaut and astronauts from 12 countries, including 11 astronauts from ESA Member States.

Mir was the successor of Salyut-7, the last of the Salyut orbital stations, which was launched in Apr 1982 and mothballed in May 1986. With Kosmos-1686 attached, Salyut-7 had a mass of about 40 tonnes when it re-entered on 7 Feb 1991, close to the peak of solar cycle 22. The Skylab space station, which was launched in May 1973, decayed during the maximum of the preceeding solar cycle 21, and re-entered on 11 Jul 1979, with a total mass of 75 tonnes. In contrast with Mir, the re-entries of Salyut-7 and Skylab were not fully controlled. Since their orbits were quite similar to Mir, the resulting risk potentials can be compared. It will be demonstrated in the following that even massive objects, such as Mir, can be safely de-orbited, if their entry is tightly controlled.

The Mir de-orbit operations were conducted by the TsUP Mission Control Center for Rosaviakosmos, following a decision by the Russian government to conclude the mission. In Dec 2000, the de-orbiting was targeted to take place in Mar 2001. The subsequent technical activities were managed by an Interdisciplinary Mir De-Orbiting Commission, headed by Yuri Koptev. The planned concept called for a natural decay to 220 – 215 km, followed by the shaping of a descent orbit during 2 consecutive orbits, leading to a perigee in the designated splash-down target area in the Pacific Ocean. The final de-orbit boost was to take place after 2 coast orbits, using all available propellant to enter into a relatively steep, destructive descent. A modified Progress M1 vehicle was launched from Baikonur on 24 Jan 2001 to dock with Mir, and to serve as a fuel reservoir and propulsion unit for the planned de-orbit operations.

To make use of the best available information for managing the Mir de-orbit, the Russian authorities approached several international partners to initiate an exchange of operationally relevant data. A cooperation between ESA and ROSAVIAKOSMOS was initiated in Jan 2001. Subsequently, an ESA Mir De-Orbit Monitoring Group was set up, tasked to collect, screen, and distribute relevant information, and to interface with ROSAVIAKOSMOS and TsUP on one side, and with international and European agencies on the other side. ESOC was assigned a key role by this group, on grounds of their experience gained during the re-entries of Kosmos 1402 and Salyut-7. The ESOC activities in support of the Mir de-orbit will be described in more detail hereafter.

2. MIR DATA EXCHANGE

As a result of technical discussions between ROSAVIAKOSMOS and ESA, in response to a request to ESA's Director General, a data exchange agreement was signed on 23 Jan 2001, which defined the technical and managerial points of contact on both sides, and which listed the information to be contributed and received by both partners. ESOC and TsUP were assigned as technical centres through which all information should be routed. Moreover, ESOC was tasked by FGAN (Research Insti-

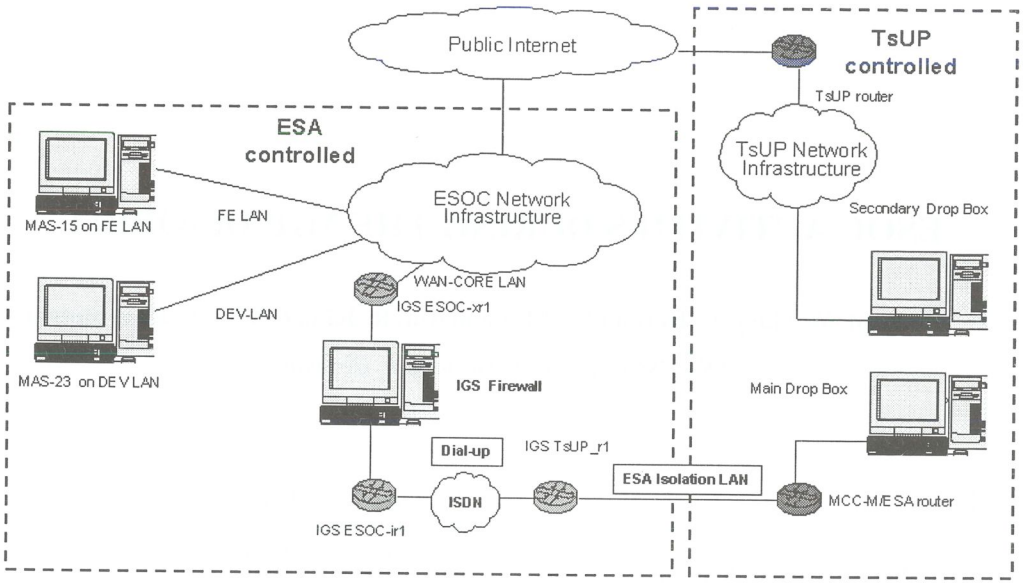

Fig. 1: Schematics of the ESOC ⇔ TsUP data exchange network during the Mir de-orbit operations.

	.tle	.osc	.bal	.rad	.ima	.pre	.act	.news
TsUP*	58	10	–	–	–	–	–	1
ESOC*	2	–	10	–	–	17	32	–
FGAN*	38	–	–	39	6	–	–	9
CNES	7	–	–	–	–	–	–	–
DGA	13	–	–	15	–	–	–	–
NASA	65	–	–	–	–	–	–	–

Tab. 1: Data received by ESOC during the Mir de-orbit, according to supplier and data type. Only data from suppliers marked as ( )* fell under the data exchange agreement. File types: *.tle → TLE data; *.osc → osculating orbit states; *.bal → ballistic parameter data; *.rad → radar tracking data; *.ima → radar imaging data; *.pre → orbit predictions; *.act → solar/geomagnetic activity forecasts; *.news → status information.

tute of High-Frequency Physics and Radar Techniques, in Wachtberg/Germany) to serve as distributor to TsUP for tracking, orbit determination, and imaging data products of FGAN's TIRA radar. The following information was to be made available to TsUP through ESOC:

- FGAN TLE data sets derived from TIRA measurements
- FGAN uncorrected range and angular tracking measurements
- ESA re-entry predictions
- ESA 27-day forecasts of solar and geomagnetic activities

The following information was to be made available to ESOC through TsUP:

- TLE data sets derived from RSSS measurements
- osculating state vectors derived from RSSS measurements
- ballistic parameter information updates
- updates on the Mir attitude
- information on planned orbit and/or attitude manoeuvres
- reports on spacecraft anomalies
- re-entry predictions

It was also agreed that ESOC should set up a reliable communication link which would allow near real-time, redundant information transfer between ESOC and TsUP, particularly during mission critical periods. Fig.1 shows the concept of the resulting network. It consists of an ESA controlled domain and a TsUP controlled domain which are connected by two redundant lines: a dial-up, high data-rate ISDN link (default connection), and a lower data-rate link via the public internet (back-up connection). The operation of the data exchange network is controlled from the ESOC side through the DISCOS database server (marked as "MAS-15"), which serves as ESA's information drop box, and which connects to the ISDN link via a firewall to access the main drop box server at TsUP. In case of a failure of the ISDN dial-up, the ESOC server directly connects to the secondary drop box at TsUP via the public internet. The primary and secondary drop boxes at TsUP are physically separate units,

not connected by a network, to be in line with security requirements of the ESA Isolation LAN used in the ISDN connection. Both TsUP drop boxes do, however, maintain identical information.

The ESOC-TsUP data exchange network was set up in January, it was tested in early February, and it went into full operation by the end of February 2001. The ESOC server MAS-15 was acting as the master machine, determining the dial-up frequency, and initiating the subsequent copy of the updated TsUP drop box information to ESOC, and of the updated ESOC drop box information to TsUP. The data exchange was running in an automatic mode, based on scripts which were triggered by the computer clock at update intervals ranging from a few hours in early March down to 3 minutes close to the Mir re-entry. The data were provided in agreed file formats, with standardised naming conventions which allowed an easy identification of the data type and its generation time. After each update, both TsUP and ESOC had a complete image of the information to date. On the ESOC side, post-processed data were automatically forwarded to the re-entry prediction workstation (marked as "MAS-23" in Fig.1), where latest information was used to update predictions which were fed back into the drop-box. ESOC's master server ("MAS-15") was also maintaining a number of additional users from ESA Member States who, under the ESA-ROSAVIAKOSMOS agreement, could monitor the information exchange and could contribute own information. Likewise, updated TLE data of Mir were received from NASA/JSC. These data, together with all other sources of TLE information (from TsUP, FGAN, CNES, DGA), were merged into an ESA-internal TLE history file, which was used to derive ballistic parameter information, and to predict the orbit decay.

The information which was entered into the ESOC and TsUP drop-boxes was catagorised in eight different classes: (1) TLE data according to the data format and underlying orbit theory defined by USSPACECOM (notation: *.tle), (2) osculating Kepler or cartesian orbit state vectors in a mean-of-date system with UTC epoch (notation: *.osc), (3) ballistic parameter information derived from orbit fits (notation: *.bal), (4) range and angular radar measurement data for given station coordinates (notation: *.rad), (5) radar images as snapshots or animations (notation: *.ima), (6) orbit and re-entry predictions (notation: *.pre), (7) short-term solar and geomagnetic activity forecasts (notation: *.act), and (8) general news on the Mir status (notation: *.news). Tab.1 summarises the contributions to the different data categories by the participating organisations. The ESA drop box, however, was exclusively supplied with the combined ESOC and FGAN data. CNES/DGA and NASA had their own data exchange agreements with TsUP, and their inputs were processed for ESOC-internal use, only. As can be noted from Tab.1, the joint ESOC/FGAN information almost covered the entire spectrum of the expected data types. The rate at which files were entered into the TsUP and ESOC drop-boxes increase from 11 at $t_{entry} - 2d$ to 48 at $t_{entry} - 1d$. The minimum delay time of orbit data (time difference between orbit determination epoch and entry into the drop-box) was on the order of 10 minutes for FGAN, 20 minutes for TsUP, and 30 minutes for NASA. The average TLE delay times, however, were somewhat larger.

3. LONG-TERM ENTRY FORECAST

In the analysis of the Mir re-entry basically three different scenarios were investigated: (1) a natural re-entry with no interfering manoeuvres, (2) a nominal, controlled de-orbit, and (3) a non-nominal de-orbit with underperformance of one or more manoeuvres. ESOC uses different prediction tools for each of these tasks, with each tool using its own orbit theory.

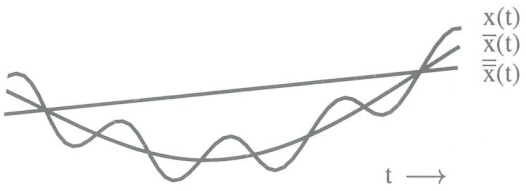

Fig. 2: Definition of osculating elements x(t), singly averaged elements $\bar{x}(t)$, and doubly averaged elements $\bar{\bar{x}}(t)$, with short-periodic, long-periodic, and secular perturbation contributions.

As input to ESOC's orbit propagators orbital elements at their determination epoch, and data on the ballistic parameter of the object are required. The orbit data are mostly available as doubly averaged mean Brouwer elements, compatible with the SGP-4/SDP-4 orbit theory, and provided in Two-Line Element (TLE) format. Such data were available for Mir from USSPACECOM, TsUP, FGAN, CNES, and DGA (ESOC also produced TLEs from FGAN measurements). TLE data often serve as a standard data exchange format, since their translation into osculating elements can be accomplished by the readily available SGP-4/SDP-4 code. Fig.2 illustrates how the transition from doubly averaged TLE states $\bar{\bar{x}}(t)$ at an epoch t is performed, by successively superimposing long-periodic contributions ($\rightarrow \bar{x}(t)$) and short-periodic spectra ($\rightarrow x(t)$). Such recovered osculating states are accurate to first order only, since the short-periodic terms in SGP-4 are limited to J_2 contributions. More precise orbital data, as required for de-orbit manoeuvre planning, and for the final descent prediction, must be obtained by directly fitting the perturbed osculating state to radar observations. This information was only available to ESOC from TsUP and from ESOC's fits to FGAN observations.

For long-term predictions of a manoeuvre-free natural re-entries ESOC uses a semi-analytical technique which propagates singly averaged orbital elements (J_2 first order means) by numerical integration of averaged perturbation equations (see ref.[6] for details). The method assumes a frozen perturbation environment over the averaging interval, performs a separation of perturbations for the averaging operation, superimposes the resulting mean time rates of change of the Kepler orbital elements (expressed in non-singular equinoctial elements), and forwards the lumped right hand sides of the perturbation equations to the numerical integrator. The following perturbations can be considered:

- geopotential: with harmonics up to degree and order 23, including $(J_2)^2$ second order terms
- airdrag: with air densities according to MSIS-77, MSIS-86, or MSISe-90 (see [3]), using 7 state pa-

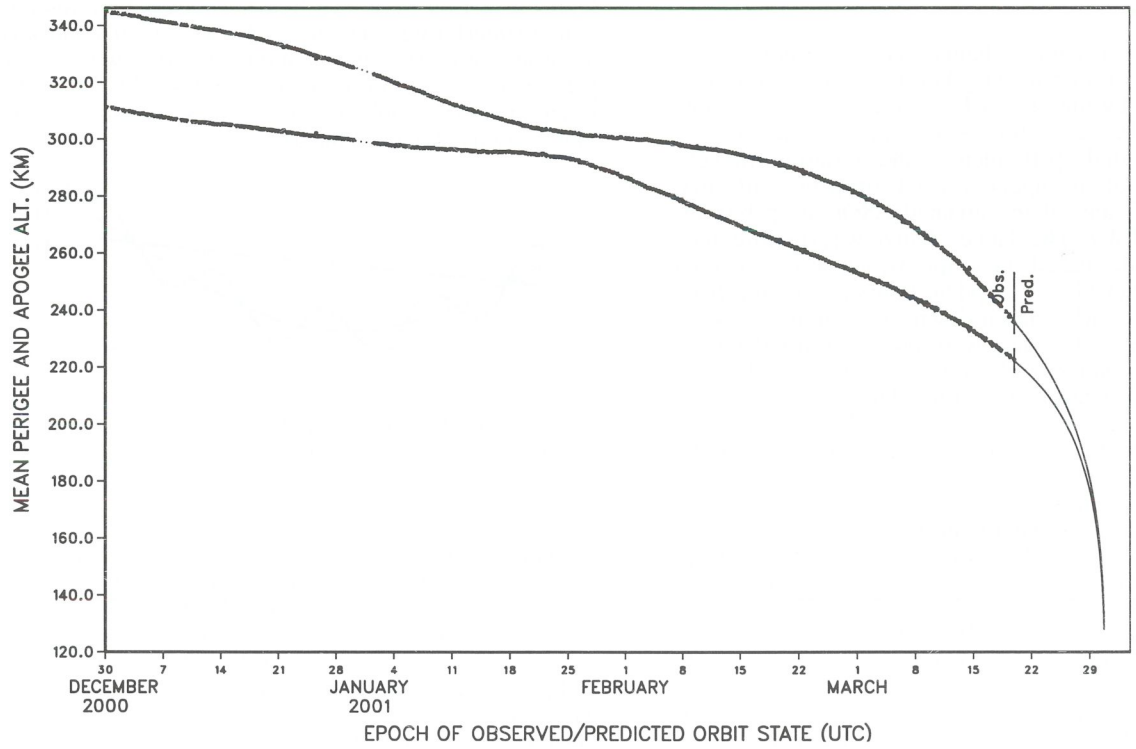

Fig. 3: Observed and predicted history of the Mir apogee and perigee altitude after 01 Jan 2001. Altitudes are based on mean semimajor axis and eccentricity, derived from TLE data (up to March 22), and predicted by ESOC (as of March 22).

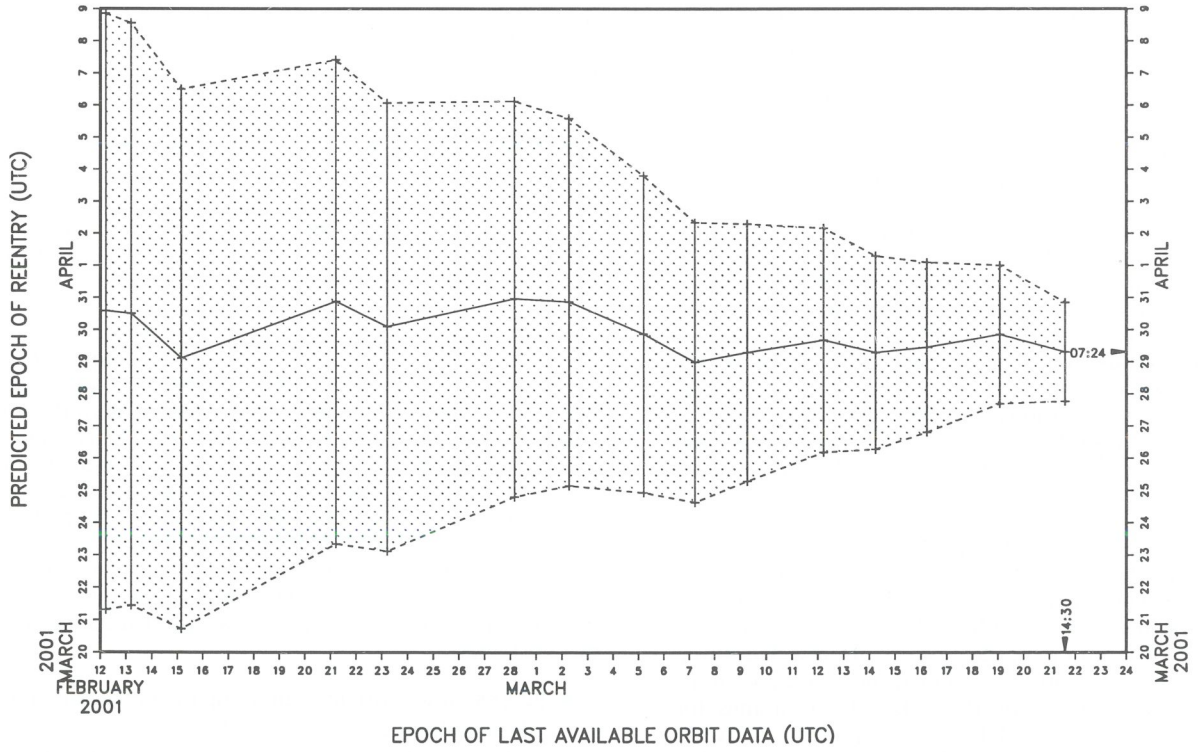

Fig. 4: Predicted date of a manoeuvre-free natural re-entry of Mir, as a function of the prediction epoch (center curve). The upper and lower curves mark the width of the re-entry time window (±20% of the remaining lifetime).

rameters; with optional winds, and harmonic cross-section variation (e.g. sun-pointing solar arrays)

- luni-solar third body: with expansions of the perturbation functions up to degree and order 23
- solar radiation pressure: including eclipses for a spherical or oblate earth; assuming a constant effective cross-section (e.g. sun-pointing solar arrays)

All perturbations are averaged independently (separation of perturbations) in a purely analytical, closed-form manner in order to determine the individual contributions to the total mean time rates of change of the Kepler state vector elements. In all cases the averaging operation is performed over an arc of 2π. of the mean anomaly M (one anomalistic revolution).

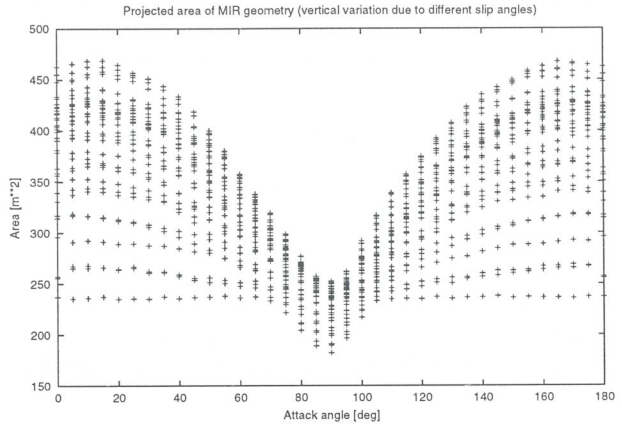

Fig. 5: Variation of the Mir aerodynamic cross-section with angle of attack (individual curves generated for side slip angles from $-90°$ to $+90°$).

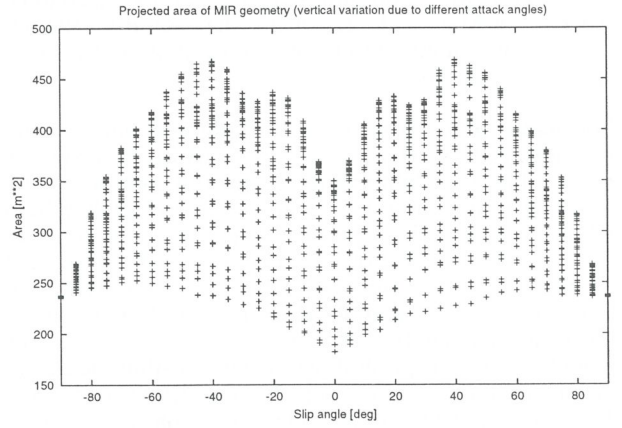

Fig. 6: Variation of the Mir aerodynamic cross-section with side slip angle (individual curves generated for angles of attack from 0° to 180°).

The integration of the averaged, perturbed equations of motion is performed by a multi-step Adams-Bashforth/Adams-Moulton predictor/corrector algorithm of user definable order (between 1 and 8), and fixed step size. The starting arc for the integration is established by a single-step Runge-Kutta/Shanks 7/8 method. As a good compromise with regard to accuracy and numerical stability, a 4-th order integrator with 2 corrector steps was used throughout the computations. During the last month of a satellites' lifetime the integration step size can decrease from several revolutions to fractions of an orbit.

For the prediction of the unlikely case of a manoeuvre-free re-entry of Mir, the described semi-analytical theory was used to retro-fit the predicted time history $a(t)$ of the semi-major axis to an observed history $a_{tle}(t)$, derived from TLE data. For this fit, the mass-to-area ratio was fixed to a mean value of $m/A = 350\,\mathrm{kg/m^2}$, and the drag coefficient c_D was adjusted by a least-squares fit to $a_{tle}(t)$. For the time span of the fitting arc solar and geomagnetic activity measurements from NOAA were used as inputs to the MSISe-90 atmosphere model. In the time period from March 2 to March 21 ($t_{entry} - 1\mathrm{d}$), 9 fits of c_D were performed, over time intervals ranging from $\Delta t = 11\mathrm{d}$ on March 2 to $\Delta t = 5\mathrm{d}$ on March 21. Each of these arcs covered 60 to 70 TLE reference states. The fitted drag coefficients were all within $c_D = 2.214 \pm 0.043$ (i.e. within $\pm 2\%$). The resulting rms residuals on the semimajor axis ranged from $\Delta a_{rms} = 70\mathrm{m}$ to 135m, while the altitude decay within the fitted time interval was on the order of 13 to 20 km. For the derived c_D, and for the adopted m/A ratio, the corresponding, mean cross-sectional area was $\bar{A} = 385\mathrm{m}^2$ (assuming a mass of 135 tonnes). This value of $\bar{A}$ matches well with the possible ranges depicted in Fig.5 and Fig.6 as function of the angle of attack and side slip angle. After March 6, Mir started a rotation about its Y-axis (Kvant-2/Spectr) with a period of $T_y \approx 6$ min, which was superimposed on an already existing rotation at $T_x \approx 20$ min about the X-axis (Kvant/Core-Module). This rotation led to an averaging of the effective cross-sectional area. The results of the ballistic parameter $B = c_D A/m$ were applicable throughout the free-molecular flight regime of Mir, until the start of the de-orbit sequence on March 23.

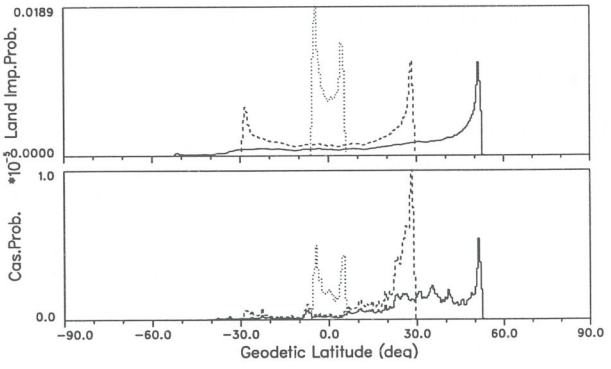

Fig. 7: Latitude dependent land impact probability and casualty probability for a near-circular orbit at inclination 51.6° (Mir, Skylab, Salyut-7), 28.5°, and 5.0°. A casualty cross-section of $10\mathrm{m}^2$ is assumed for the surviving fragments.

The predictions of a natural re-entry of Mir stabilized in mid February around March 30 $\pm$ 1 day. The final long-term prediction, using a TLE state from 2001/03/21 14:31 UTC, indicated a natural re-entry on 2001/03/29 07:24 UTC $\pm$ 37 h. At that time, Mir had a mean perigee of 213 km (decaying at -3.7 km/d), and a mean apogee of 225 km (decaying at -5.2 km/d).

The long-term risk assessment for the Mir entry can only be done on grounds of the latitude dependent distribution of land impact probability, and the resulting casualty probability. For the Mir orbit inclination of 51.6°, and for an assumed 10m^2 effective cross-section of survivor fragments, Fig.7 shows the corresponding results (note: casualty probabilities can be scaled with the effective cross-section). The land impact probability is 27.2%, and the casualty probability is on the order of 1 in 7,570. Most of the land impact probability, and almost all of the casualty probability is concentrated in the northern hemisphere (since only 33.3% of the land masses and 11.7% of the population are in the southern hemisphere). Consequently, most designated de-orbit areas, including the one of Mir, are located south of the equator, mostly below latitudes of 30°S. The splash-down zone into which Mir was to be de-orbited is indicated in Fig.7, in the South Pacific Ocean.

4. SHORT-TERM ENTRY FORECAST

In the final phase of the Mir lifetime the orbit propagation was handed over from a semi-analytical procedure to a numerical integration, which used a single-step Runge-Kutta/Shanks 7/8 process with controlled step-size to integrate the perturbed, osculating cartesian orbit state vector (see Fig.2) in a mean-of-date system, using the following perturbation contributions:

- geopotential GEM-T1 with harmonics up to degree and order 36
- airdrag, with air densities according to MSISe-90 [3], patched with Jacchia-Lineberry densities below 180 km [8], and with drag coefficients adjusted with changes of the flight regime
- luni-solar third body attraction
- solar radiation pressure, including eclipses for an oblate earth
- orbit manoeuvres, assuming impulsive ΔV's

For all non-gravitational forces a constant mass-to-area ratio of $m/A = 350\,\text{kg/m}^2$, was adopted, with an initial drag coefficient of $c_D = 2.2$ for the aerodynamic perturbations. The c_D coefficient was adjusted with the changing aerodynamic flight regime, from free-molecular, via transitional, to continuum. Using analytical solutions for simple shapes (sphere, cylinder, circular plate) in free-molecular flow (as $c_D = \text{fct}(\text{Kn}_\infty)$) and continuum flow (as $c_D = \text{fct}(\text{Ma}_\infty)$), and using Kn_∞ dependent bridging functions for the transitional regime. During the final descent of Mir (starting at 215 km altitude), the drag coefficient dropped by 10% each, when passing the altitude marks 110 km, 30 km, 26 km, and 20 km. It finally attained a value of $c_D = 1.18$ at the time of impact, while Mir was traveling at 61 m/s.

The density model(s) used NOAA observations and 27 day nominal ESOC forecasts of solar and geomagnetic activity indices [10]. Calibration computations for several historic re-entries indicated that the MSISe-90 atmosphere model had systematic density deficiencies at altitudes between 110 km (the turbo-pause) and 180 km, which resulted in local underpredictions of the drag force by up to 40%. This can probably be attributed to the analytical concentration profiles which are used in MSISe-90, and which are matched to observed number densities at higher altitudes by adjusting the initial conditions at the turbo-pause. This shortcoming was removed by a smooth fairing between MSISe-90 densities at 180 km (and above) and Jacchia-Lineberry densities at 120 km (and below). Since the Jacchia-Lineberry model is a derivative of the Jacchia-71 model (= CIRA-72 for thermospheric altitudes), it is largely based on in-situ drag measurements, and it hence tends to be more reliable in this altitude regime, which determines the final re-entry trajectory.

The strategy which was elaborated by the TsUP Mission Control Centre for the Mir de-orbit focused on 3 separate burns during 4 consecutive orbits. By definition, orbit #1 should be the first groundtrack with a geographic longitude of its ascending node West of 20° E. Each subsequent orbit would have a westward groundtrack shift by about 22.2° (see Fig.9).

ESOC's analysis concentrated on the following scenario:

- burn #1 on orbit #15, at orbit position $u = 40°$, with an equivalent, impulsive $\Delta V = -7.7$ m/s, opposite to the transversal direction
- burn #2 on orbit #16, with the same characteristics as for burn #1
- burn #3 on orbit #02, with the same characteristics as for burn #1, but with an equivalent, impulsive $\Delta V = -20.3$ m/s

This de-orbit scenario was recurring on a daily basis, with a slight drift in nodal longitude by roughly -1.5°/d. Based on the long-term forecast of the Mir altitude decay, using last TLE data from March 16, the decision altitude for initiating the de-orbiting sequence was expected to be reached on March 21, 22, or 23, depending on the acceptable minimum altitude, and depending on the atmospheric conditions.

For the de-orbit sequence several failure scenarios could be envisaged, of which two were analysed by ESOC in more detail: (1) a total failure of the orbit control system, resulting in a natural decay, and (2) an incomplete burn #3 due to a propellant shortage. Case (1) would have resulted in an uncontrolled re-entry on March 29, around noon UTC. This result was fairly stable from March 16 onwards. Case (2) is illustrated in Fig.8. Depending on the achieved magnitude of burn #3, a ΔV of 17 to 20.2 m/s would result in a splash-down location within the designated target area, while a performance between 15.2 and 15.8 m/s could lead to an impact location in the northern hemisphere and possibly in Europe. For an effective ΔV of only 10 m/s, 5 m/s, or even 0 m/s, the on-orbit dwell time would be extended to approximately 5 hours, 20 hours, and 40 hours, with no possibility to control the impact footprint. Due to a thorough preparation and flawless execution of the Mir de-orbiting sequence by the TsUP control staff, none of these contingency cases occurred.

The actual de-orbit sequence which was finally implemented by TsUP is summarised in Tab.3. On March 22, at 01:05 UTC, one day prior to the planned de-orbit, an

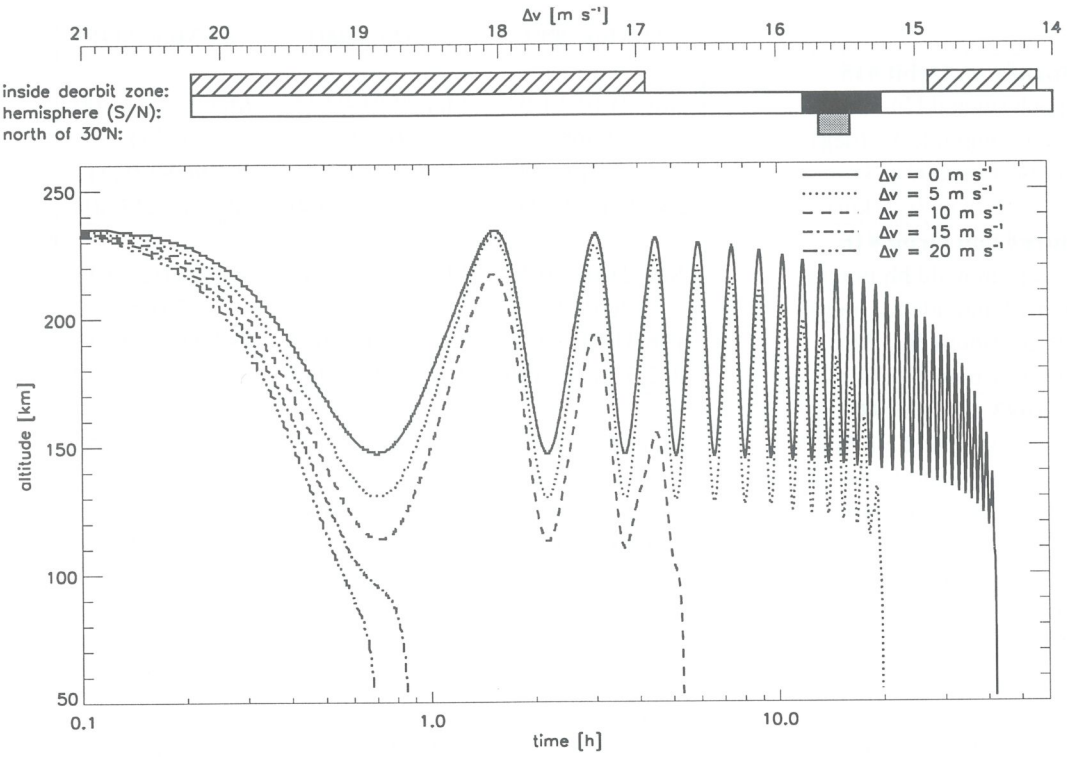

Fig. 8: Sensitivity analysis of an underperformance of de-orbit burn #3 on orbit #02 (impulsive ΔV at $u = 40°$ assumed). The horizontal bar charts indicate, as a function of the applied ΔV, if the splash down location is inside the target area (hatched bar, see also Fig.9), if it's inside the South or North hemisphere (white/black bar), or if it's at mid-latitudes of the North Hemisphere (grey bar).

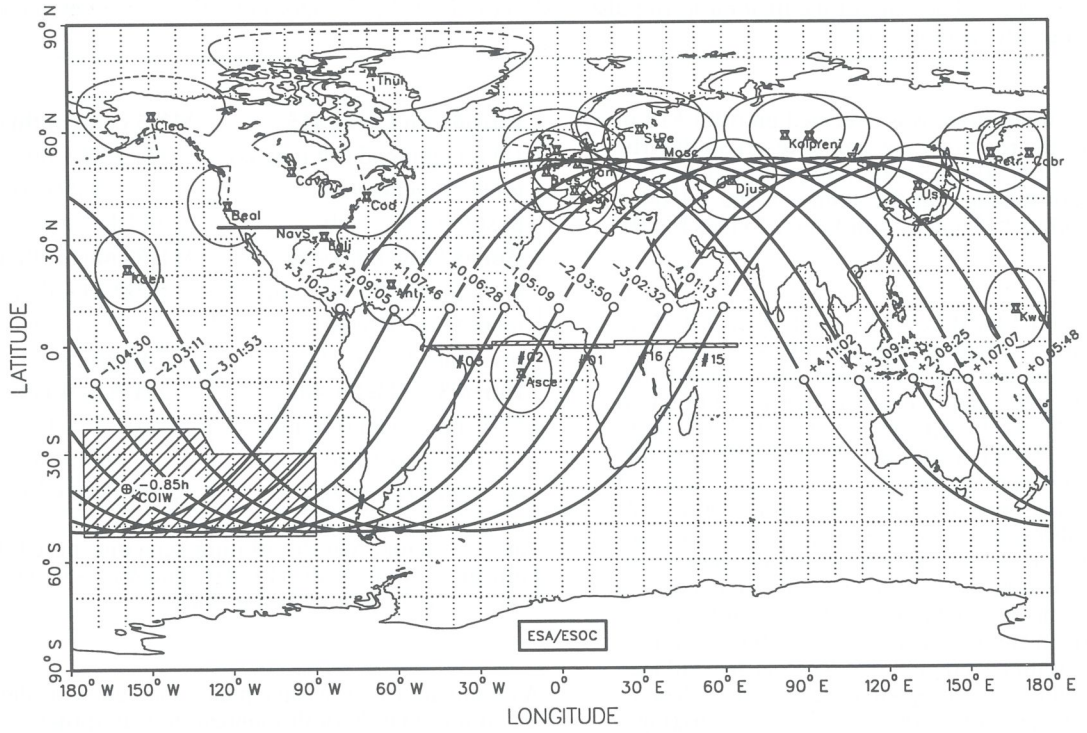

Fig. 9: The Mir de-orbiting scenario. - COIW marks the "centre of impact window" as predicted by ESOC for a 3-burn strategy on orbits #15, #16, and #02. The hatched area marks the designated de-orbit zone in the South Pacific Ocean.

	21-Mar-2001	22-Mar-2001	23-Mar-2001
Burn#1 on Orbit #15			
epoch (mon.dd hh:mm:ss)	Mar.21 01:21:05	Mar.22 01:02:15	Mar.23 00:42:00
nodal longitude λ_N (deg)	62.565	60.879	59.541
pre/post-burn H_{pe} (km)	214.424/196.480	210.953/192.602	206.963/188.217
pre/post-burn H_{ap} (km)	231.161/222.996	226.622/218.889	221.117/213.808
Burn#2 on Orbit #16			
epoch (mon.dd hh:mm:ss)	Mar.21 02:49:40	Mar.22 02:30:45	Mar.23 02:10:25
nodal longitude λ_N (deg)	40.019	38.353	37.036
pre/post-burn H_{pe} (km)	196.314/171.671	192.413/167.630	187.972/163.011
pre/post-burn H_{ap} (km)	222.520/221.185	218.354/217.183	213.205/212.242
Burn#3 on Orbit #02			
epoch (mon.dd hh:mm:ss)	Mar.21 05:46:20	Mar.22 05:27:15	Mar.23 05:06:45
nodal longitude λ_N (deg)	-4.949	-6.574	-7.851
pre/post-burn H_{pe} (km)	171.212/104.051	167.048/99.860	162.238/95.014
pre/post-burn H_{ap} (km)	219.500/218.796	215.224/214.613	209.928/209.431
splash-down location λ/ϕ (deg)	-41.75/-22.31	-126.62/-50.59	-159.21/-39.57
splash-down UTC time	07:00:58	06:24:38	05:57:58
Burn#3 on Orbit #03 (back-up)			
epoch (mon.dd hh:mm:ss)	Mar.21 07:14:40	Mar.22 06:57:00	Mar.23 06:34:50
nodal longitude λ_N (deg)	-27.434	-29.038	-30.273
pre/post-burn H_{pe} (km)	170.845/103.670	166.620/99.420	161.856/94.604
pre/post-burn H_{ap} (km)	218.639/217.956	214.220/213.630	208.736/208.275
splash-down location λ/ϕ (deg)	-73.91/-31.90	-153.68/-49.78	+176.55/-38.43
splash-down UTC time	08:26:03	07:52:05	07:25:38

Tab. 2: ESOC results of different Mir de-orbiting scenarios, based on a 3-burn strategy on orbits #15, #16, and #02 (see Fig.9), with orbit #03 as back-up for the final burn. Impulsive ΔV's of -7.7 m/s, -7.7 m/s and -20.3 m/s are assumed to be applied at orbit positions of $u = 40°$.

attitude control manoeuvre was executed on orbit #15 in order to reduce the rotation rates and to re-orient the Mir station to an inertial attitude with a proper line-up of the Progress control thrusters at the centre of the intended thrust arcs on orbits #15 and #16 on March 23 (see Fig.9).

The de-orbit burn #1 (March 23, 00:31:50 to 00:53:32 UTC, on orbit #15) had a total ΔV of -9.27 m/s. It moved the perigee location by almost 180° towards the southern hemisphere, and reduced the perigee altitude to 188 km. Burn #2 on the subsequent orbit #16 (02:00:24 to 02:24:28 UTC) generated a ΔV of -10.4 m/s, and further reduced the perigee altitude to 156 km. Both of these manoeuvres only used the combined Progress attitude control thrusters. Orbit #01 was used as coast arc to do orbit determination, and to align the Progress main engine for the final burn arc, which should be centred at about 90° from the ascending node. The de-orbit burn of the Progress main engine started at 05:07:26 UTC, on orbit #02, well within coverage of the Russian surveillance network. The burn was completed successfully, close to the time of coverage loss, at 05:27:02 UTC, generating a total ΔV of -28.0 to 28.5 m/s, which placed the perigee altitude close to 80 km, and led to a nominal re-entry location at 40°S and 160°W. This outcome closely matches ESOC's predictions for the March 23 scenario as summarised in Tab.2, and as illustrated in Fig.9.

Burn#1 on Orbit #15	**M1-5 control thrusters**
UTC begin/end (hh:mm:ss)	00:31:59 – 00:53:32
total ΔV generated	$-9.27\,\mathrm{m/s}$
post-burn $H_{pe} \times H_{ap}$	$188.0\,\mathrm{km} \times 213.5\,\mathrm{km}$
Burn#2 on Orbit #16	**M1-5 control thrusters**
UTC begin/end (hh:mm:ss)	02:00:24 – 02:24:28
total ΔV generated	$-10.4\,\mathrm{m/s}$
post-burn $H_{pe} \times H_{ap}$	$156.1\,\mathrm{km} \times 213.2\,\mathrm{km}$
Burn#3 on Orbit #02	**M1-5 main engine**
UTC begin/end (hh:mm:ss)	05:07:36 – 05:27:02
total ΔV generated	$-28.0\,\mathrm{m/s}$
post-burn $H_{pe} \times H_{ap}$	$\approx 80.0\,\mathrm{km} \times 213.0\,\mathrm{km}$

Tab. 3: Actual Mir de-orbiting scenario, based on a 3-burn strategy on orbits #15, #16, and #02 (see Fig.9). All times are in UTC on 23-Mar-2001.

As compared with earlier plans, the centre of the thrust arc of the final de-orbit manoeuvre was shifted by about +45° towards the northernmost point of orbit #02, and the ΔV magnitude was larger than anticipated. These two effects combined resulted in a steeper descent trajectory towards the planned splash-down zone in the South Pacific, with a safe altitude clearance during the pass over

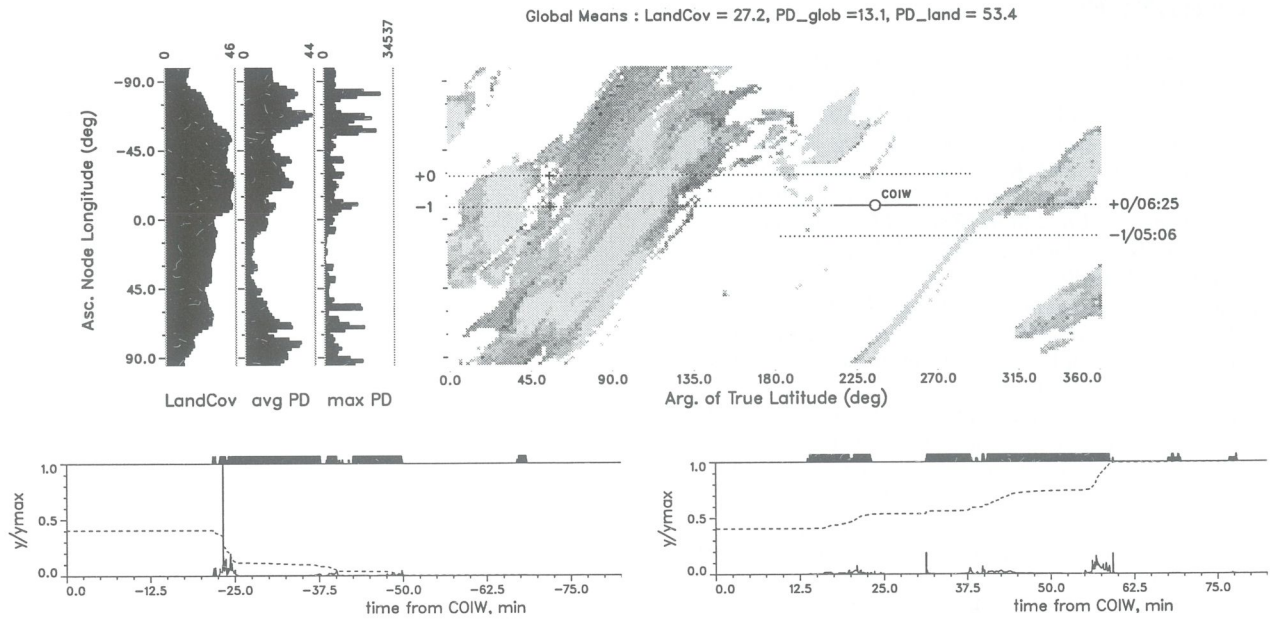

Fig. 10: Mir impact footprint area of ±2,550 km100 km, indicated by a solid line in the top chart, and centred on the reconstructed impact location (COIW, see also Fig.9). The bottom charts show the land coverage (black siluette) and the normalised local population density (solid line), and resulting cumulated risk (dashed line) in up-track (left) and down-track direction (right).

China, Korea and Japan. The associated on-ground risk is illustrated in Fig.10. The top chart shows a map of the world population density vs. geographic longitude of ascending node and argument of true latitude of the Mir orbit, with ±1 orbit groundtrack overlaid, centered on the predicted impact location. The left-hand strip charts provide the land coverage, average population density, and maximum population density for each node position of a Mir orbit. The chosen entry groundtrack has a maximum possible land coverage for this orbit inclination of 51.6°. Also the mean and max. population density of this orbit are at about 50% of the possible maxima. This averaged information is resolved in up-track and down-track direction in the bottom charts, over a time interval of ±80 minutes (land masks are indicated by black siluettes on top). The largest risk contribution according to these charts would result from the pass over northern China and Korea. The decision by TsUP to delay the final de-orbit manoeuvre, and to use a large ΔV, is consistent with a minimisation of the on-ground risk, due to a safe altitude clearance of densely populated areas. Using a conservative assumption of a 2σ dispersion of the Mir impact footprint by ±2,500 km along-track and ±100 km cross-track, centred at 40°S and 160°W, the assessed residual risk to human life on ground due to the Mir re-entry was virtually zero.

5. SUMMARY AND CONCLUSIONS

The Mir de-orbit campaign was a good example of open information exchange and technical cooperation between several international space agencies during an event of common concern. As such, it was following in the footsteps of a traditionally good collaboration between TsUP and ESOC, which was established during the re-entry of Salyut-7. The data and information exchange during the Mir campaign, however, had a new quality. For the first time, ESOC was serving as an international data reception and distribution centre, with secure, high-rate data links to and from TsUP, and with fast turn-around orbit updates by TsUP, FGAN, NASA, and CNES/DGA. The ESOC/TsUP drop-box system, which was designed within a short time span, and which worked flawlessly in an unattended, automated mode, throughout the Mir campaign, might also be used during future international campaigns, or in multi-lateral cooperations.

The close technical cooperation, with the Russian colleagues in particular, largely contributed to the transparency of the Mir de-orbit planning and operations, and hence allowed to make a realistic assessment of possible contingencies, and of residual risks.

The absolutely nominal performance of the complex Mir de-orbiting procedure was the consequence of a thoroughly planned and professionally executed end-of-lifetime spacecraft disposal.

ACKNOWLEDGEMENTS

The authors wish to acknowledge the support to ESOC, provided during the Mir de-orbit campaign in particular by the TsUP Mission Control Center (Korolev/RU), the Research Institute for High Frequency Physics and Radar Techniques (FGAN/FHR, Wachtberg/D), the company Hypersonic Technologies Goettingen (Lindau/D), NASA-JSC (Houston/USA), CNES (F), and DGA (F).

REFERENCES

[1] Dreher, P.E., Little, R.P., and Wittenstein, G., *Skylab Orbital Lifetime Prediction and Decay Analysis*, NASA Technical Memorandum 78308, 1980

[2] Fritsche, B., Roberts, T., Romay, M., Ivanov, M., Grinberg, E., and Klinkrad, H., *Spacecraft Disintegration During Uncontrolled Atmospheric Re-Entry*, proceedings of the Second European Conference on Space Debris, ESA SP-393, pp. 581–586, Darmstadt, 1996

[3] Hedin, A., *Extension of the MSIS Thermosphere Model into the Middle and Lower Atmosphere*, Journal of Geophysical Research, Vol.96, No.A2, pp. 1159-1172, Feb 1991

[4] Kerridge, D., Carlaw, V., and Beamish, D., *Development and Testing of Computer Algorithms for Solar and Geomagnetic Activity Forecasting*, ESA contract report, ESA CR(P) 3039, 1989

[5] Klinkrad, H., *Long-Term Analytical Decay and Re-Entry Prediction*, proceedings of an International Workshop on the Re-Entry of Space Debris, ESA SP-246, pp. 39–48, Darmstadt, 1985

[6] Klinkrad, H., *Salyut-7/Kosmos-1686 Re-Entry Prediction Activities at ESOC*, proceedings of an International Workshop on the Salyut-7/Kosmos-1686 Re-Entry, ESA SP-345, pp. 17–34, Darmstadt, 1991

[7] Klinkrad, H., *Evolution of the On-Ground Risk During Uncontrolled Re-Entries*, paper IAA-99-IAA.6.7.05, 50th IAF Congress, Amsterdam/The Netherlands, 1999

[8] Mueller, A., *Jacchia-Lineberry Upper Atmosphere Density Model*, NASA Report 82-FM-52/JSC-18507, Oct 1982

[9] Rex, D., *Re-Entry of Large Satellites into the Earth Atmosphere - Risk and Prediction* (in German), Journal of Flight Sciences and Space Research (ZFW), Vol.4, No.6, pp. 354–366, 1980

[10] Thompson, A., Clark, T., and Kerridge, D., *Computer Algorithms and Fortran Programs for Forecasting Solar and Geomagnetic Activity in the Short-Term*, ESA contract report, 1992

[11] Tobler, W., Deichmann, U., Gottsegen, J., and Maloy, K., *The Global Demography Project*, Technical Report TR-95-6, National Center for Geographic Information and Analysis, Dept. of Geography, University of California, Santa Barbara/CA, Apr 1995